Sensor and Simulation Notes

Note 348

3 November 1992

KEY FORMULAS FOR APPLYING GTD TO STRIP LIKE STRUCTURES

Prof. Y.Rahmat-Samii
Department of Electrical Engineering, UCLA. Los Angeles, CA

Abstract

In this note, some of the key equations required to apply the construction of GTD technique to strip type structures are presented. The motivation has been to collect these equations for their possible application to TEM-fed paraboloidal reflector antennas. In particular, to provide design considerations on the effects of the strip-type blockage on the performance of TEM-fed reflector antennas. It is worth mentioning that care must be exercised in applying GTD to narrow structures and for non-ray field incidence. It should also be noticed that GTD application would be more applicable for wide angle pattern determination than the boresight and main beam performance characterization.

Contents

Section		Page
1.	Introduction	3
	1.1 Summary of key GTD Equations	3
2.	A Representative Example	8
	2.1 Geometrical Optics	8
	2.2 Geometrical Theory of Diffraction	9
	2.3 Uniform Theory of Diffraction	11
	References	13

ACKNOWLEDGEMENT

We are thankful to Capt.L.Miner and Dr.Carl E. Baum of Phillips Laboratory for their guidance and encouragement.

1. Introduction

TEM-fed reflector antennas have received much attention [1-4] as viable radiators for ultrawideband applications. Figure 1 demonstrates potential design configurations. The triangular feed plates allow for the generation of the spherical TEM waves which are then scattered from the paraboloidal reflector surface. In this note, our objective is to summarize some of the key equations required to apply GTD construction for the determination of the effects of the TEM launchers (strips) on the antenna performance. An example is provided to guide the reader about how the GTD construction may be used in computing the diffracted field from strip-type structures.

1.1 Summary of key GTD Equations

Figure 2 provides an insight into the basic philosophy of applying GTD. The most important aspects are the notions of " **Localization** ", " **Ray field** ", " **Canonical Problems** ", " **Reflection and Diffraction Points** ", " **Reflection and Diffraction Coefficients** " etc. The key equations necessary to apply the GTD construction to perfectly conducting edge-type structures are presented in Tables 1 to 4. Additional details of relating to these equations may be found in [5].

Typically, after the incident ray field is identified, one determines the reflection and diffraction points based on the laws of reflection and diffraction and then construct the geometrical optics and diffracted fields. For the TEM-fed reflector antennas, one may make the assumption that the field exiting the reflector has plane wave characteristics which can readily be cast into the form of a ray field. The problem is then to investigate the diffraction characteristics of the illunminating ray field off the strip launchers. Obviously, attention must be given to the polarization characteristics of the illuminating ray field. This procedure is useful under the assumption that the widths of the strips are several wavelengths long. Additionally, if one wants to obtain more accurate results, it may become necessary to consider multiple diffractions across the width of the strip.

Furthermore, it is anticipated that the GTD construction should provide good accuracy for estimating wide angle performance by essentially combining the diffracted fields with those of the direct radiation from the reflector. However, near the main beam region, extra care must be exercised if caustics are formed.

In the next section, we provide a representative example in constructing the GTD solution for the diffracted field from a rectangular plate. The example should assist the reader in applying the GTD formulation and appreciate the underlying aspects of its implementation.

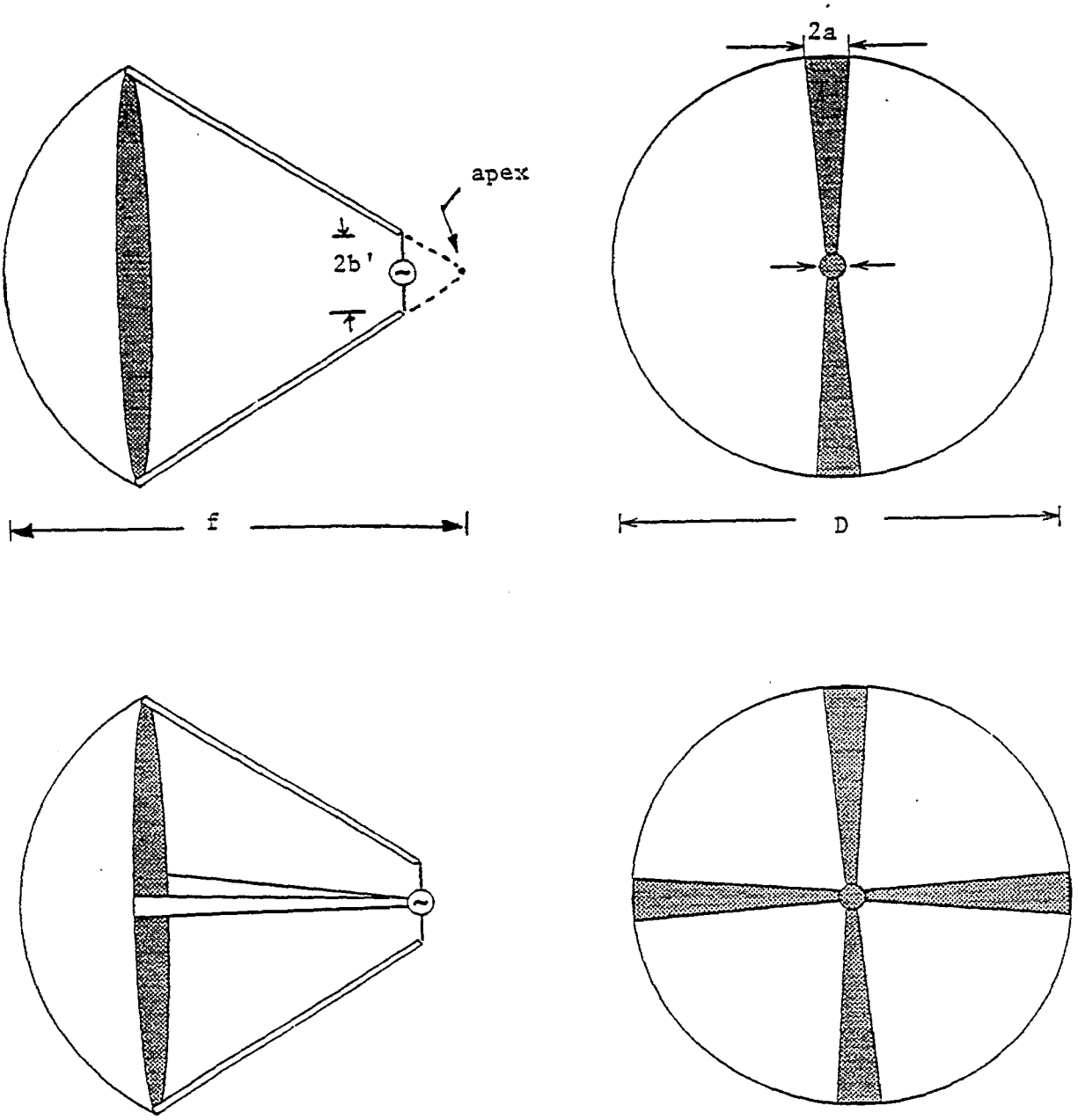

Figure 1.1 Antenna Configurations for two-arm and four-arm TEM-fed reflectors

from **Maxwell's Equations to GTD Solutions**

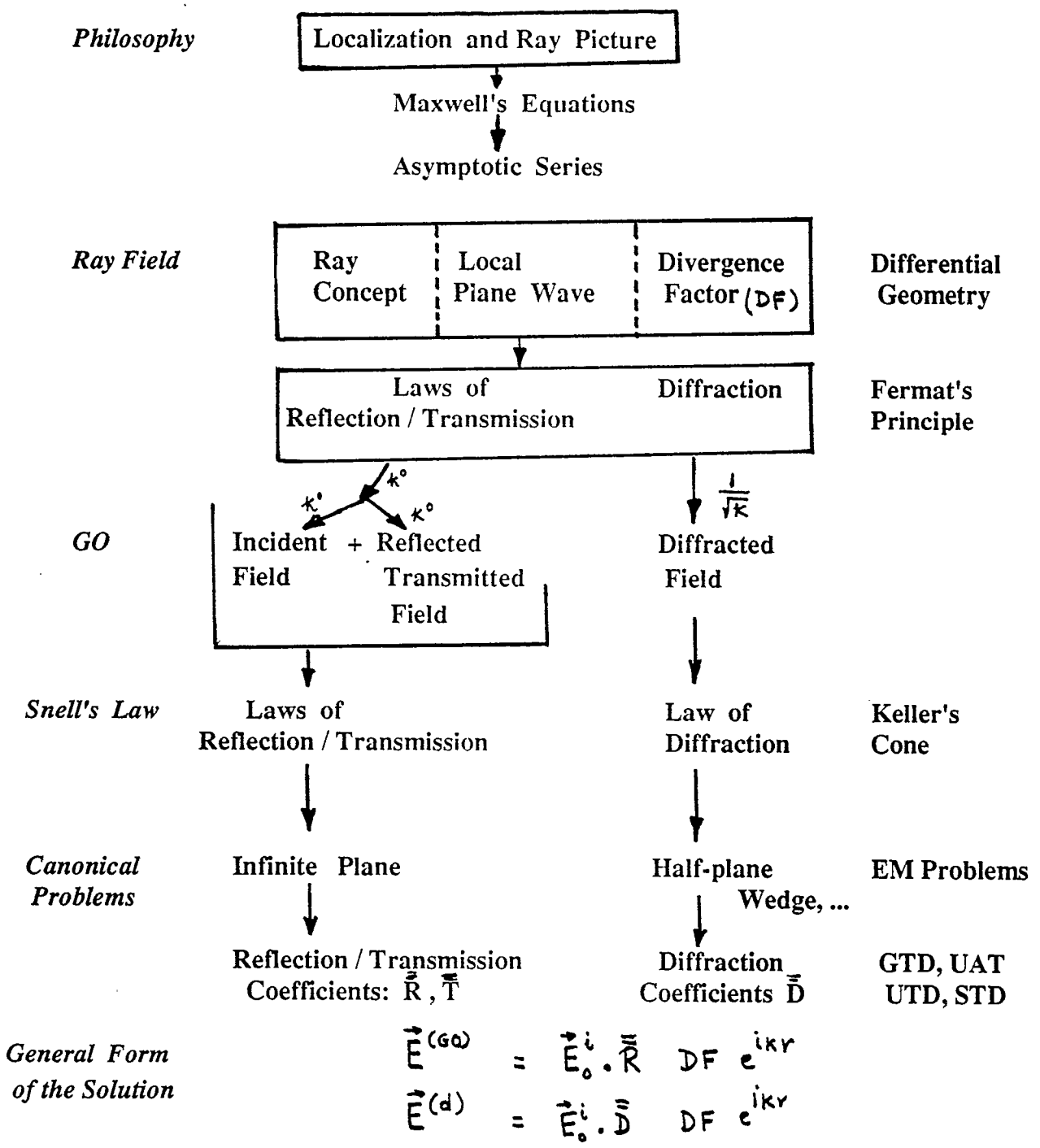

Figure 2. A block diagram highlighting the main features of implementing GTD construction

Summary of Keller's Diffraction

TABLE 1. **Total Field**

geometrical optics **diffracted**

$$\vec{E}^t(\vec{r}) = \Theta(\varepsilon^i)\ \vec{E}^i(r) + \Theta(\varepsilon^r)\ \vec{E}^r(r) + \vec{E}^d(r)$$

$$\vec{E}^d(r) \quad k^{-(1/2)}\ \exp(ikS^d(r) \sum_{m=0}^{\infty} (-ik)^{-m}\ \vec{e}_m^d\ (\vec{r}) \quad , \quad k \to \infty$$

Keller's Theory gives for the dominant term (m=0)

$$\vec{E}^d(r) = \frac{\exp(ik\sigma^d)}{\sqrt{k\sigma^d}} \frac{1}{\sqrt{1 + \sigma^d/R_1^d}} \quad \vec{\vec{D}}\ \vec{E}^i(\sigma_1^i = \sigma_2^i = \sigma^i = 0) + O(k^{-3/2})$$

σ^d = path length along the diffracted ray from the diffraction point

TABLE 2. **Curvature of Diffracted Wavefront**

$$R_2^d = 0$$

$$\frac{1}{R_1^d} = \frac{1}{R^i(\Omega^i)} + \frac{\kappa}{\sin^2(\Omega^i)} \left(\hat{n} \cdot \hat{\sigma}^i - \hat{n} \cdot \hat{\sigma}^d \right)$$

where

$$\frac{1}{R^i(\Omega^i)} = \frac{\cos^2(\Omega^i)}{R_1^i} + \frac{\sin^2(\Omega^i)}{R_2^i}$$

R_1^i , R_2^i = principal radii of incident wavefront passing through diffraction point O

Ω^i = angle measured (toward $\hat{\sigma}_2^i$) from $\hat{\sigma}_1^i$ to the projection of $\hat{t}$ on $\hat{\sigma}_1^i$ $\hat{\sigma}_2^i$ plane

κ = curvature of edge Γ at point O (non-negative)

β^i = angle measured from

n = unit normal at edge Γ at O

$\hat{\sigma}^i$, $\hat{\sigma}^d$ = direction of incident (diffracted) rays

TABLE 3. **Divergence Factor**

$$DF = \frac{1}{\sqrt{1 + \sigma^d / R_1^d}}$$

positive real value or negative imaginary value

TABLE 4. **Keller's Diffraction Coefficient for an edge (spherical coordinates):**

$$\bar{\bar{D}} \equiv \bar{\bar{D}}^{(sp)} = \frac{\exp(i\pi/4)}{2\sqrt{2\pi}\sin(\beta^i)} \begin{bmatrix} \chi^i + \chi^r & 0 \\ 0 & \chi^i - \chi^r \end{bmatrix}$$

where

$$\chi^{i,r} = (-1)^{\varepsilon^{i,r}} \left| \csc \frac{\alpha^d + \alpha^i}{2} \right|$$

$$= (-1)^{\varepsilon^{i,r}} \csc \left| \frac{\text{angle between } S^d \text{ and } S^{i,r} \text{ in } (t_1, t_2) \text{ plane}}{2} \right|$$

2. A Representative Example

2.1 Geometrical Optics

The geometry of the problem of interest is shown in Figure3.A source is placed on the z axis at a height h above the center of perfectly conducting rectangular plate of dimensions $2a$ by $2b$. It is assumed that the plate is large enough that the GO/GTD construction may be used to determine the far-field radiation pattern for this configuration.

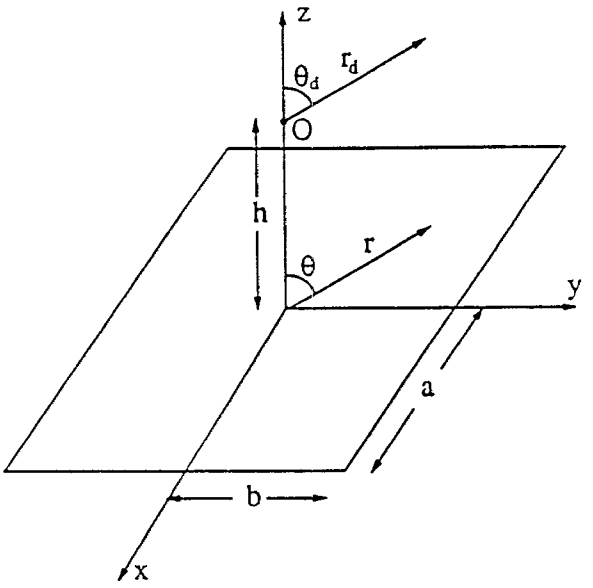

Figure3: Geometry for the dipole over the perfectly conducting plate.

With $e^{-i\omega t}$ time variation assumed and suppressed, an infinitesimal dipole located at $z = h$ and oriented along the z axis radiates a ray field expressed as

$$\vec{E}^i = E_o \sin\theta_d \frac{e^{ikr_d}}{r_d}\hat{\theta}_d \tag{1}$$

where r_d and θ_d are shown in Figure 3. To determine the GO field for this source, we express the dipole field in Eq. (1) in terms of r and θ as defined in Figure 3 and construct its image as if the ground plane were infinite in extent. Since we are observing in the far-field, we use the well known far-field approximation for amplitude and phase variations with distance. In this case, the dipole radiation pattern is given by

$$\vec{E}^{dip} = E_o \sin\theta \frac{e^{ik(r-h\cos\theta)}}{r}\hat{\theta} \tag{2}$$

while the image source has a radiation pattern

$$\vec{E}^{img} = E_o \sin\theta \frac{e^{ik(r+h\cos\theta)}}{r}\hat{\theta}. \tag{3}$$

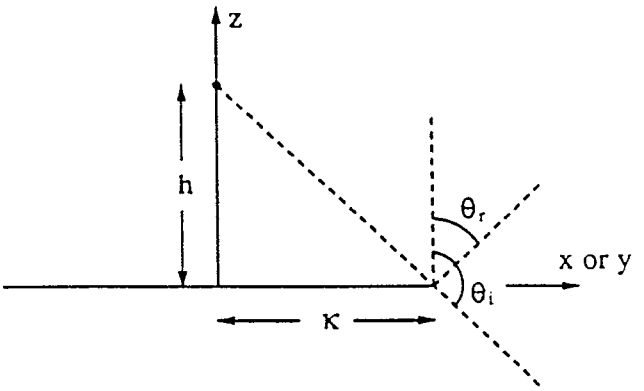

Figure 4: Incident and reflected shadow boundaries for GO fields.

Consistent with the asymptotic approximation, we construct the GO field by superimposing the fields from the dipole and its image, making the appropriate provisions for the incident and reflected shadow boundaries. Figure 4 shows the geometry of these shadow boundaries for the principal planes. In this figure and for the rest of this report, the distances a and b will be represented by

$$\kappa = \begin{cases} a & \text{if } \phi = 0 \\ b & \text{if } \phi = \pi/2 \end{cases} .$$

Using the expressions in Eqs. (2) and (3) we obtain

$$\vec{E}^{go} = E_o \sin\theta \frac{e^{ikr}}{r} \left[e^{ikh\cos\theta} \mathcal{U}(\theta_r - \theta) + e^{-ikh\cos\theta} \mathcal{U}(\theta_i - \theta) \right] \hat{\theta} \tag{4}$$

where $\theta_r = \arctan(\kappa/h)$ and $\theta_i = \pi - \theta_r$. In this representation, $\mathcal{U}(x)$ denotes the unit step function. Eq. (4) represents the total GO field for any observation angle θ in the two principal planes.

2.2 Geometrical Theory of Diffraction

The field expression of Eq. (4) is a first order asymptotic approximation to the total field for large plate dimensions. The presence of the unit step functions implies discontinuous behavior at the shadow boundaries which is physically impossible for this geometry. An improvement to this result is obtained by adding the next dominant term in the asymptotic expansion of the fields. The use of the GTD construction provides a method for accomplishing this.

To determine the field diffracted by the plate edges, it is necessary to locate the diffraction points that will contribute to the far-field in the x-z and y-z planes. The dominant contribution to this field results from diffraction at the points $(\pm a, 0, 0)$ in the x-z plane and $(0, \pm b, 0)$ in the y-z plane. The Keller's cone at these points becomes a plane coincident with the observation plane. It should be noted that diffraction from the edges at $y = \pm b$ will produce some field in the x-z plane. However, if the height h is small compared with the

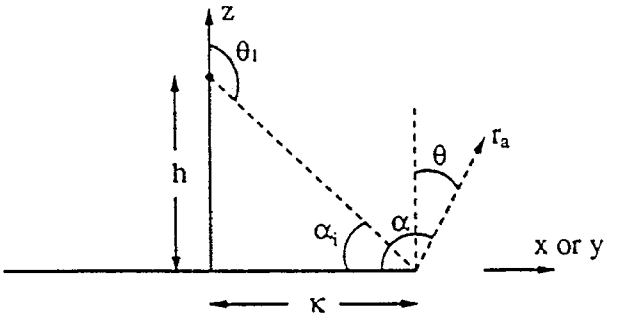

Figure 6: Incident and reflected shadow boundaries for GO fields.

plate dimensions, this contribution is negligible when compared to the dominant diffraction mechanism discussed above.

Following the GTD construction, the diffracted field contribution to the far-field in the principal observation planes can be determined. Since the incident wavefront is assumed to be spherical, the principal radii of curvature of the front at the diffraction point are given by

$$R_1^i = R_2^i = \sqrt{\kappa^2 + h^2}. \tag{5}$$

Using this result with the fact that the curvature of the plate edges is zero allows us to write the principal radii of curvature of the diffracted wavefront as

$$R_1^d = \sqrt{\kappa^2 + h^2} \tag{6}$$

$$R_2^d = 0. \tag{7}$$

The divergence factor of the diffracted wavefront can now be determined from

$$DF = \frac{1}{\sqrt{1 + r_a/R_1^d}} = \frac{1}{\sqrt{1 + r_a/\sqrt{\kappa^2 + h^2}}} \tag{8}$$

where r_a is defined in Figure 6. Since we are observing in the far-field region with $r \gg \kappa$, we will let $r_a = r$.

The diffraction coefficients must next be determined. Using the geometry of Figure 6, we may write

$$\chi_i = -\sec\frac{(\alpha - \alpha_i)}{2} \tag{9}$$

$$\chi_r = -\sec\frac{(\alpha + \alpha_i)}{2} \tag{10}$$

$$\alpha_i = \arctan h/\kappa. \tag{11}$$

Since the polarization of the incident field is orthogonal to the tangent along the plate edge at the diffraction point, the diffraction coefficient for the wavefront is merely the sum of χ_i and χ_r given above. This is known as the coefficient for the hard polarization and may be expressed as

$$D^h(\alpha) = \chi_i + \chi_r = -\sec\frac{(\alpha - \alpha_i)}{2} - \sec\frac{(\alpha + \alpha_i)}{2}. \tag{12}$$

The relations in Eqs. (8) and (12) allow us to construct the diffracted field for a given incident field.

Making use of Eq. (1) with the appropriate modification for r and θ and from the geometry of Figure 6, we can express the strength of the incident field at the diffraction point as

$$E^i = E_o \frac{\sin\theta_1}{\sqrt{\kappa^2+h^2}} e^{ik\sqrt{\kappa^2+h^2}} = E_o \frac{\kappa}{\kappa^2+h^2} e^{ik\sqrt{\kappa^2+h^2}}. \tag{13}$$

Now, making use of the rotation operator to determine the polarization of the diffracted components in the far-field and adding the contribution from both edges of the plate, we obtain the general expression of the field for the observation planes $\phi = 0$ and $\phi = \pi/2$

$$\vec{E}^d = E_o \frac{\kappa e^{i\pi/4} e^{ik(r+R)}}{2R^2\sqrt{1+r/R}\sqrt{2\pi kr}} \left[D^h(\theta+\pi/2)\, e^{-ik\kappa\sin\theta} - D^h(\psi)\, e^{ik\kappa\sin\theta} \right] \hat{\theta} \tag{14}$$

where

$$\psi = \begin{cases} \pi/2-\theta & \text{if } 0 \le \theta \le \pi/2 \\ 5\pi/2-\theta & \text{if } \pi/2 \le \theta \le \pi \end{cases}$$

$$R = \sqrt{\kappa^2+h^2}.$$

In Eq. (14), the first diffraction coefficient is for diffraction from the point at x or $y = +\kappa$ and the second is for diffraction from the point at x or $y = -\kappa$. Also, the far-field approximation has been used for magnitude and phase variations with r.

Making use of the previous GO result of Eq. (4), the total field radiated by the dipole-plate geometry is then constructed as the sum of the GO and GTD contributions of the field as

$$\vec{E}^t = \vec{E}^{go} + \vec{E}^d. \tag{15}$$

Since the pattern in Eq. (14) is symmetric about the z axis, Eq. (15) gives the expression for the total field anywhere in the principal planes.

2.3 Uniform Theory of Diffraction

When the observation angle θ is near the value of the shadow boundary angles θ_i and θ_r, the GTD diffraction coefficients become singular. In order to compute the fields in these transition regions, the Uniform Theory of Diffraction (UTD) is used. In this methodology, the singularity in the diffracted field is remedied by altering the diffraction coefficients. This procedure requires that near the incident shadow boundary the coefficient χ_i be replaced by

$$\tilde{\chi}_i(\alpha) = -\sec\frac{(\alpha-\alpha_i)}{2} \frac{F(|\xi^i|)}{\hat{F}(|\xi^i|)} \tag{16}$$

where

$$\xi^i = \sqrt{2kR}\cos\frac{(\alpha-\alpha_i)}{2}$$

$$F(x) = \frac{e^{-i\pi/4}}{\sqrt{\pi}} \int_x^\infty e^{it^2} dt$$

$$\hat{F}(x) = \frac{e^{i(x^2+\pi/4)}}{2x\sqrt{\pi}}$$

and R is defined below Eq. (14). Similarly near the reflected shadow boundary, the coefficient χ_r is replaced by

$$\tilde{\chi}_r(\alpha) = -\sec\frac{(\alpha+\alpha_i)}{2}\frac{F(|\xi^r|)}{\hat{F}(|\xi^r|)} \tag{17}$$

where

$$\xi^r = \sqrt{2kR}\cos\frac{(\alpha+\alpha_i)}{2}.$$

Note that F and $\hat{F}$ are the Fresnel integral and its first asymptotic term, respectively. Placement of these diffraction coefficients in the expression of Eq. (14) for observation points near the incident and reflected shadow boundaries removes the singularity and provides a smooth field variation in the transition regions.

References

[1] C.E.Baum, "Radiation of Impulse-Like Transient Fields, " Sensor and Simulation Note 321, November 1989.

[2] C.E.Baum, " Configurations of TEM Feed for an IRA, " Sensor and Simulation Note 327, 27 April 1991.

[3] E.G.Farr, " Analysis of the Impulse Radiating Antenna, " Sensor and Simulation Note 329, 24 July 1991.

[4] E.G.Farr, " Prepulse Associated with the TEM Feed of an Impulse Radiating Antenna, " Sensor and Simulation Note 337, March 1992.

[5] D-W. Duan, Y.Rahmat-Samii and J.P.Mahon, "Scattering from a Circular Disk: A Comparitive Study of PTD and GTD Techniques, " Proceedings of the IEEE, vol.79, no.10, October 1991, pp 1472-1480.